Abbas, S. A., Barlow, J. J., & Matta, K. L. (1983b) *Carbohydr. Res. 112*, 201–211.
Bergh, M., & Van den Eijnden, D. H. (1983) *Eur. J. Biochem. 136*, 113–118.
Brockhausen, I., Rachaman, E. S., Matta, K. L., & Schachter, H. (1983a) *Carbohydr. Res. 120*, 3–16.
Brockhausen, I., Williams, D., Matta, K. L., Orr, J., & Schachter, H. (1983b) *Can. J. Biochem. Cell Biol. 61*, 1322–1333.
Brockhausen, I., Orr, J., & Schachter, H. (1984) *Can. J. Biochem. Cell Biol. 62*, 1081–1090.
Carlsson, H. E., Sundblad, G., Hammarstrom, A., & Lonngren, J. (1978) *Carbohydr. Res. 64*, 181–188.
Carver, J. P., & Grey, A. A. (1981) *Biochemistry 20*, 6607–6616.
Distler, J. J., & Jourdian, G. W. (1978) *Methods Enzymol. 50*, 514–520.
Dixon, M., & Webb, E. C. (1964) *The Enzymes*, 2nd ed., pp 84–87, Longmans, London.
Flowers, H. M., & Shapiro, D. (1965) *J. Org. Chem. 30*, 2041–2043.
Hounsell, E. F., Wood, E., Feizi, T., Fukuda, M., Powell, M. E., & Hakomori, S. I. (1981) *Carbohydr. Res. 90*, 283–307.
Kurosaka, A., Nakajima, H., Funakoshi, I., Matsuyama, M., Nagayo, T., & Yamashina, I. (1983) *J. Biol. Chem. 258*, 11594–11598.
Longmore, G. D., & Schachter, H. (1982) *Carbohydr. Res. 100*, 365–392.
Lowry, O. H., Rosebrough, N. J., Farr, A. L., & Randall, R. J. (1951) *J. Biol. Chem. 193*, 265–275.
Nasir-ud-Din, Jeanloz, R. W., Vercelotti, J. R., & McArthur, J. W. (1981) *Biochim. Biophys. Acta 678*, 483–496.
Newman, W., & Kabat, E. A. (1976) *Arch. Biochem. Biophys. 172*, 535–550.
Roseman, S., Distler, J. J., Moffatt, J. G., & Khorana, H. G. (1961) *J. Am. Chem. Soc. 83*, 659–663.
Sadler, J. E. (1984) in *The Biology of Carbohydrates* (Ginsburg, V., & Robbins, P. W., Eds.). Vol. 2, pp 199–288, Wiley-Interscience, New York.
Schachter, H., & McGuire, E. J. (1968) *Fed. Proc., Fed. Am. Soc. Exp. Biol. 27*, 345.
Schachter, H., & Williams, D. (1982) in *Mucus in Health and Disease* (Chantler, E. N., Elder, J. B., & Elstein, M., Eds.) Vol. 2, pp 3–28, Plenum Press, New York.
Schachter, H., McGuire, E. J., & Roseman, S. (1971) *J. Biol. Chem. 246*, 5321–5328.
Slomiany, A., & Slomiany, B. L. (1978) *J. Biol. Chem. 253*, 7301–7306.
Slomiany, B. L., Murty, V. L., & Slomiany, A. (1980) *J. Biol. Chem. 255*, 9719–9723.
Stellner, K., Saito, H., & Hakomori, S. (1973) *Arch. Biochem. Biophys. 155*, 464–472.
Tsuji, T., Yamamoto, K., Konami, Y., Irimura, T., & Osawa, T. (1982) *Carbohydr. Res. 109*, 259.
Van Halbeek, H., Dorland, L., Vliegenthart, J. F. G., Hull, W. E., Lamblin, G., Lhermitte, M., Boersma, A., & Roussel, P. (1982) *Eur. J. Biochem. 127*, 7–20.
Williams, D., & Schachter, H. (1980) *J. Biol. Chem. 255*, 11247–11252.
Williams, D., Longmore, G. D., Matta, K. L., & Schachter, H. (1980) *J. Biol. Chem. 255*, 11253–11261.
Wu, A. M., Kabat, E. A., Nilsson, B., Zopf, D. A., Gruezo, F. G., & Liao, J. (1984) *J. Biol. Chem. 259*, 7178–7186.

Tryptophan Imaging of Membrane Proteins†

A. M. Kleinfeld
Department of Physiology and Biophysics, Harvard Medical School, Boston, Massachusetts 02115
Received June 12, 1984

ABSTRACT: A theoretical analysis of resonance energy transfer between protein tryptophan and the *n*-(9-anthroyloxy) (AO) fatty acid probes has been carried out to evaluate its potential use in determining the tryptophan distribution in membrane proteins. The Förster theory for two-dimensional energy transfer was formulated to calculate multiple donor (tryptophan) transfer efficiencies to ensembles of AO probes at different depths in the bilayer. The variation of transfer efficiency with AO probe depth is found to be a sensitive function of tryptophan position and the protein radius but not the dipole–dipole orientation factor or the decay heterogeneity of the donor. For single tryptophan-containing proteins the model predicts that the tryptophan position can be determined with a precision of about 2 Å. Although for multiple tryptophans there is appreciable deterioration in resolution, it is still possible to determine the essential features of the distribution such as its first two moments. The positions determined by this method are the projections of the tryptophan positions on a plane perpendicular to the membrane surface, since the probes distribute uniformly around the protein. To analyze the data, a Monte Carlo approach has been developed to search for tryptophan distributions compatible with the observed efficiencies and to display the results in terms of a tryptophan density map. It is shown that even for cases in which little is known about the quantum yield distribution, significant information can be determined about the tryptophan spatial distribution.

Determination of the structure of membrane proteins is one of the most challenging problems in molecular biology. With few exceptions relatively little is known about the tertiary structure of proteins within the membrane. Tertiary structure information has been obtained for bacteriorhodopsin by combining the results of diffraction studies of the crystalline purple membrane, the primary structure, and theoretical arguments (Henderson & Unwin, 1975; Khorana et al., 1979; Ovchin-

† This work was supported by Grant PCM-830268 from the National Science Foundation. This work was done during the tenure of an Established Investigatorship (87-174) of the American Heart Association, and funds were contributed in part by the Massachusetts affiliate.

0006-2960/85/0424-1874$01.50/0

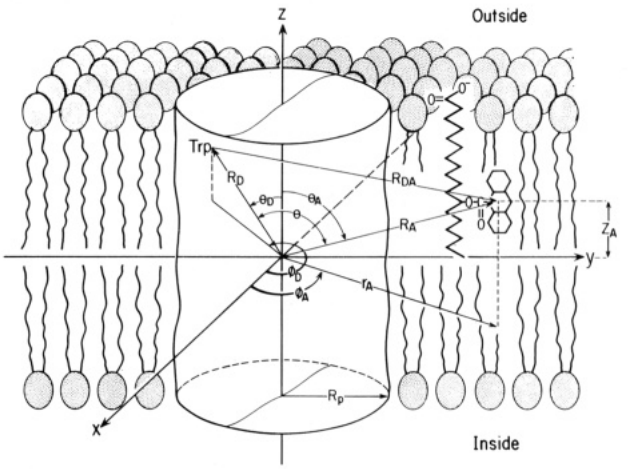

FIGURE 1: Membrane protein model and the tryptophan–AO geometry. The origin of the coordinate system is the intersection of the protein Z axis and the midplane (xy) of the lipid bilayer. R_D,θ_D,ϕ_D and R_A,θ_A,ϕ_A are the spherical coordinates of the donor (tryptophan) and acceptor (AO), respectively. Z_A is the z coordinate of a particular acceptor, and r_A is the projection of R_A on the xy plane.

nikov et al., 1979; Engelman et al., 1980, 1982). Although there will probably be considerable progress in crystallizing membrane proteins, the problem of how the protein is organized in the membrane will remain. Present resolution (about 7 Å) for the two-dimensional membrane crystals is not sufficient to resolve individual residues. Methods, therefore, that determine the location of particular residues, in situ, will be invaluable for understanding membrane protein structure. In the present study it is shown that resonance energy transfer between tryptophan residues of a membrane protein and a series of membrane probes, the *n*-(9-anthroyloxy) fatty acids (AO), can be used to obtain information about the spatial distribution of tryptophan residues. Since relatively low concentrations of these probes are needed, it is possible to investigate proteins in physiologically relevant configurations.

Overview of the Model. As seen in Figure 1, the membrane is envisioned to contain essentially one protein, represented to a first approximation by a uniform cylinder of radius R_p. The location of a particular tryptophan residue can be specified by appropriate radial and angular coordinates. In a typical experiment one of eight different AO probes is added to a suspension of membrane vesicles. The probe intercalates with its carboxyl terminus anchored in the lipid head-group region and with its AO moiety buried a distance Z_A from the midplane of the bilayer. The critical energy-transfer distance (R_0) for the tryptophan–AO pair is between 20 and 24 Å, and therefore, transfer measurements between the tryptophan and the ensemble of AO acceptors provide information about structures whose characteristic radii are between 10 and 40 Å.

The AO probes form an ensemble of acceptors located within the plane of the membrane. Energy transfer, therefore, between a single tryptophan and this ensemble yields an average tryptophan–AO separation, weighted by the surface distribution of the AO probes. It is possible, however, to determine more than simply the mean tryptophan–AO separation since the different AO probes form a set of virtually identical acceptors, differing primarily in their Z_A position. If measurements with at least two different probes are performed, triangulation may be used, in effect, to determine the location of the tryptophan. The probes distribute uniformly around the protein, so that only two tryptophan coordinates can be determined. Hence, all tryptophans at a depth z, on a locus formed by a ring of radius r, yield equivalent energy-transfer efficiencies. The two coordinates (r, z) of the set of equivalent tryptophans can be represented by the projection of the ring on the (y, z) plane through the protein.

Table I: Transmembrane Location of the *n*-AO Probes[a]

n-AO	ΔR[b]	ΔR[c]	ΔH[d]	ΔR[e]	R[f]
2					19.0
3				1.1	17.9
6		4	8	4.6	14.4
7				5.7	13.3
9			12.0	8.0	11.0
10					9.9
12	12.2	8	13.0	11.4	7.6
16			14.0	16.0	3.0

[a] Values are in angstroms, and ΔR values are relative to 2-AO. [b] The NMR study of Podo & Blasie (1977), in which the probe positions were determined relative to the methylene positions of the lipid acyl chains. R was evaluated by assuming that the acyl chain is all trans and therefore the C–C bond length is 1.53 Å. [c] Energy transfer to hemoglobin in whole red cells (Eisinger et al., 1982). [d] Energy transfer to hemoglobin in whole red cells (Eisinger & Flores, 1982). [e] CPK models in the extended configuration. [f] The absolute R values were obtained by assuming that the fatty acid acyl chain is all trans (1.53-Å C–C length) and that 2-AO is located 19 Å from the bilayer midplane. Justification for this assumption is provided by the R values in the table and by studies which suggest that the probe position varies smoothly with depth in the bilayer (Chalpin & Kleinfeld, 1983).

To deal with multiple tryptophan-containing proteins, it is necessary to evaluate energy transfer from the ensemble of tryptophan donors to the ensemble of AO acceptors. The average energy-transfer efficiency of the donor ensemble is determined by a quantum yield weighted sum of the individual tryptophan to AO ensemble efficiencies. The pattern formed from the ensemble averaged energy-transfer efficiencies as a function of the AO position is quite sensitive to the tryptophan distribution, although the spatial resolution of this distribution depends upon how completely the tryptophan quantum yield distribution is known. An approximate distribution which retains the essential features of the actual one can very often be determined even if only the average tryptophan quantum yield is known.

THEORY

A number of studies have applied the two-dimensional theory of Förster (1948) to geometries that involve axial symmetry about the donor (Shaklai et al., 1977; Fung & Stryer, 1978; Koppel et al., 1979; Wolber & Hudson, 1979; Dewey & Hammes, 1980; Estep & Thompson, 1979). In this section we will outline the two-dimensional energy-transfer theory and elaborate on the changes needed to accommodate the geometry of our model. We first enumerate the important assumptions and restrictions used in the model.

(i) It is assumed that both the proteins and AO acceptors are uniformly distributed within the plane of the membrane. The protein may form specific oligomeric associations; however, these oligomeric states must themselves be uniformly distributed.

(ii) It is assumed that in the course of a measurement the probes remain in the outside half of the bilayer. Hence, the inside/outside partition factor is zero.

(iii) Probe depth or Z_A values were adopted by consideration of the results of several studies including X-ray diffraction (Lesslauer et al., 1972), NMR (Podo & Blasie, 1977), energy transfer (Eisinger & Flores, 1982), and CPK models of the probes. Values for Z_A from these studies and the adopted values are shown in Table I.

(iv) The bilayer surface is treated as a plane, an assumption justified by the work of Fung & Stryer (1978) and Eisinger et al. (1981).

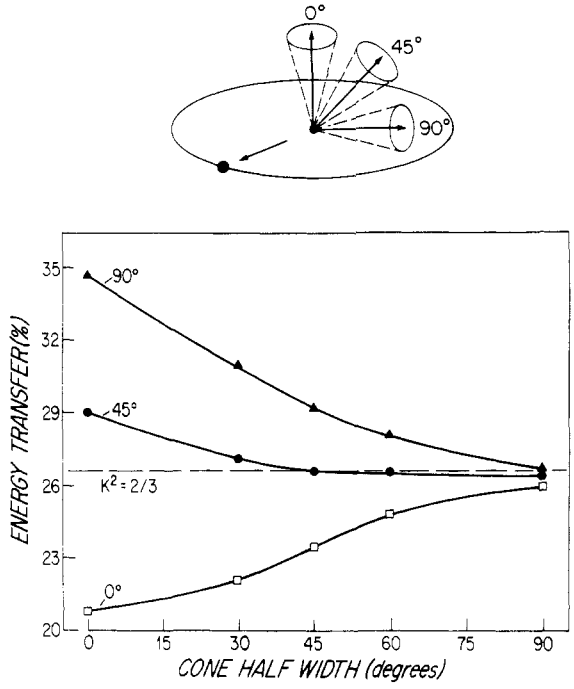

FIGURE 2: Energy-transfer efficiency as a function of the donor orientation. T values were calculated as a function of the donor cone width for three orientations of the cone axis by using the method described in the supplementary materials. For the calculation depicted here the tryptophan donor was located at the center of a cylinder of a radius of 20 Å, the acceptor Z_A was set to zero, and other parameters are the same as in Figure 5. The value indicated by the dashed line was determined by assuming that the tryptophan is isotropic ($K^2 = {}^2/_3$).

(v) A dipole–dipole orientation factor (K^2) equal to ${}^2/_3$ is used. The results of calculations in the supplementary material (see paragraph at end of paper regarding supplementary material) and Figure 2 indicate isotropy ($K^2 = {}^2/_3$) is a good approximation.

(vi) Two forms of tryptophan heterogeneity are considered: the heterogeneity of the fluorescence intensity decay of a single tryptophan and the quantum yield heterogeneity of different residues in a multi-tryptophan protein (site heterogeneity). Decay heterogeneity is discussed in the supplementary material where it is shown that, for a coupled two-state decay, the energy-transfer efficiency is insensitive to the decay constants. Site heterogeneity is a more important issue. Two models will be considered: one in which the quantum yields of all tryptophans are identical and one in which only the average quantum yield is known.

Single Donor Theory. The decay of the donor tryptophan in the model system of Figure 1 can be described by the rate equation

$$dP_i(t)/dt = -(k_i + \sum_{i,j} k_{ij}^T)P_i(t) \quad (1)$$

In this equation $P_i(t)dt$ is the probability that the ith donor (tryptophan) is excited at a time between t and $t + dt$ following a pulse of exciting light, k_i is the decay rate in the absence of energy transfer ($k_i = 1/\tau_i$), and k_{ij}^T is the resonance energy-transfer rate from the ith donor to the jth acceptor. In the weak coupling limit of Förster's theory

$$k_{ij}^T = (1/\tau_i)(R_0^i/R_{ij})^6 \quad (2)$$

R_{ij} is the distance between the ith donor and jth acceptor. (When there is no explicit sum over the i and j indexes we will often exchange i and j with D and A for the sake of clarity.) The critical transfer radius R_0^i (in cm) of the ith tryptophan is given by

$$R_0 = [(8.785 \times 10^{-25})K^2 Q_i J/n^4]^{1/6} \quad (3)$$

in which Q_i is the quantum yield of the ith donor in the absence of acceptor, and n is the index of refraction of the medium between donor and acceptor. The overlap integral J is defined as

$$J = \int \epsilon_A(\lambda) f_i(\lambda)\lambda^4 \, d\lambda \quad (4)$$

in which $\epsilon_A(\lambda)$ is the acceptor molar extinction coefficient density at wavelength λ, $f_i(\lambda)$ is the corrected fluorescence intensity of the donor, normalized so that the integral of $f_i(\lambda)$ over its emission band equals Q_i. The orientation factor K^2 between a particular donor (we have dropped the i subscript for clarity) and a particular acceptor is given by

$$K^2 = (\sin \xi_D \sin \xi_A \cos \gamma - 2 \cos \xi_D \cos \xi_A)^2 \quad (5)$$

in which ξ_D and ξ_A are the angles between the $\vec{R}_{DA}$ (radial vector between donor and acceptor) and the donor and acceptor dipole directions, respectively, and γ is the azimuthal angle between donor and acceptor dipoles.

In applying this description to the model system of Figure 1, we have assumed that the donor molecules are uncoupled and, therefore, eq 1 holds separately for each donor. It is also assumed that the concentration of excited tryptophan is negligible compared to the ground-state population. If in addition the K_{ij}^T values are independent of time (the dynamic average regime is applicable), then the solution to eq 1 for a particular acceptor configuration (positions and dipole orientation) is

$$P_i(t) = P_i(0) \exp[-t(1/\tau_i + \sum_j k_{ij}^T)] \quad (6)$$

The ensemble average of eq 6 over all possible acceptor configurations is given by

$$\langle P_i(t) \rangle = \int P_i(t,\{A\}) W\{A\} \, d\{A\} \quad (7)$$

in which $W\{A\}$ is the probability density of a particular distribution of acceptors, $\{A\}$. In particular, if we assume that the probes are uniformly distributed, then in the geometry of Figure 1, $W\{A\}d\{A\} = (r_A - R_D \sin \theta_D \cos \omega)dr_A d\phi_A/(\text{area available to acceptor})$. It follows that the ensemble average can be expressed [see, e.g., Fung & Stryer (1978)] as

$$\langle P_i(t) \rangle = \exp(-t/\tau_i) \exp[-\sigma L(t)] \quad (8)$$

$$L(t) = \int_0^{2\pi} \int_{R_m}^{\infty} [1 - \exp[(-t/\tau_i)(R_0^i/R_{DA})]^6](r_A - R_D \sin \theta_D \cos \omega)dr_A d\phi_A$$

in which σ is the two-dimensional number density of acceptor molecules and R_m is the radial integration parameter (at the depth Z_A). The radial integration parameter is the distance between the protein surface and the center of the acceptor molecule; it is equal to the protein radius (R_p) plus the acceptor radius. Since the acceptors are not necessarily axially symmetric about each donor, we use the geometry of Figure 1 to express R_{DA}^2 as

$$R_{DA}^2 = r_A^2 + z_A^2 + R_D^2 - 2R_D(Z_A \cos \theta_D + r_A \sin \theta_D \cos \omega) \quad (9)$$

in which R_D is the radial, θ_D and ϕ_D are the angular coordinates of a particular tryptophan residue, and $\omega = \phi_A - \phi_D$.

Orientation Factor. Energy transfer depends on the relative orientation of the donor and acceptor dipoles. This orientation is difficult to determine experimentally, and the uncertainties in K^2 may lead to considerable ambiguity in the determination of R_{DA}. The effect of donor–acceptor orientation on resonance energy transfer has been carefully analyzed in the papers of Dale & Eisinger (1975) and Dale et al. (1979). These studies

demonstrated that for a donor–acceptor pair at a fixed $\vec{R}_{DA}$, limits can be placed on the uncertainty in K^2 by measurements of the donor, acceptor, and transfer depolarization factors. In a protein containing several tryptophans, however, the individual donor and transfer depolarization factors cannot readily be determined. Furthermore, since the AO acceptors are distributed throughout the plane of the membrane, they form an ensemble of $\vec{R}_{DA}$ values, each of which has a different orientation factor with respect to any single donor. Thus, it is not possible to use the method of Dale et al. (1979) to set limits on the variation of energy-transfer efficiency due to uncertainty in the donor–acceptor orientation, since a single averaged K^2 cannot be defined.

Any degree of motional freedom will significantly reduce the effect of the orientation factor. In the present case the lack of donor–acceptor correlation leads to a considerable reduction in the K^2 sensitivity of the ensemble averaged energy-transfer expressions. In liposomes formed from several different phosphatidylcholines above the phase transition ($r_\infty < 0.05$), and in vesicles of red cell ghosts ($r_\infty < 0.13$) the anthroyloxy group exhibits rapid and almost unrestricted rotation at any position on the acyl chain (A. M. Kleinfeld, unpublished observations; Kutchai et al., 1984). Even in liposomes below the gel to liquid-crystalline phase transition, it appears that the rotation of the AO probes is relatively unhindered (Vincent et al., 1982). Mixed absorption dipoles of the acceptor also yield more isotropic K^2 values (Hass et al., 1978). In the case of the AO acceptors the absorption band in the region which is overlapped by tryptophan emission (~300–380 nm) is a mixture of orthogonal dipoles (Matayoshi & Kleinfeld, 1981). Taken together, the mixed polarization absorption bands and the lack of appreciable rotational constraints suggest that the acceptor is well described by an unrestricted isotropic rotor.

The orientational constraints of the tryptophan are more difficult to assess. For single tryptophan-containing proteins, fluorescence measurements can be performed to determine the dipole rotation rate and motional restriction. Most of these results suggest considerable motional freedom on the nanosecond time scale (Ross et al., 1981a; Lakowicz & Weber, 1980; Munro et al., 1979; Lakowicz et al., 1983). On the other hand, some fluorescence and NMR measurements do suggest restrictions in certain cases (Ross et al., 1981b; Munro et al. 1979; Kinsey et al., 1981; Gall et al., 1982; Lakowicz et al., 1983).

Since experimental information about the dipole orientation and restriction cannot generally be obtained in multi-tryptophan proteins, it is essential to estimate, by calculation, the degree of uncertainty due to restrictive motion of the tryptophan dipole. To obtain this estimate, the dynamic average of K^2 was evaluated as a function of $\vec{R}_{DA}$ for a model in which the donor is confined to a solid cone and the acceptor is an isotropic rotor. This dynamic average, computed with the geometry of Figure 1, was then used to determine the energy-transfer efficiency averaged over the acceptor positions as a function of the donor's orientation parameters. [A similar approach was used by Koppel et al. (1979) and Eisinger et al. (1981) for geometries different than the present one.] Results of these calculations, shown in Figure 2 and in the supplementary material, demonstrate that variation in energy-transfer efficiency about the value obtained for isotropic donor–acceptor pairs ($K^2 = {}^2/_3$) is less than 25%, even in the case of completely immobilized tryptophan. For tryptophan with sufficient motional freedom to undergo diffusive motion within a cone of 30° half-width, the uncertainty in the efficiency reduces to 10%. Since this is the same order as the experimental uncertainties, $K^2 = {}^2/_3$ will be used in what follows.

Multiple Donor Energy Transfer. The extension of the theory to multiple tryptophan is accomplished by evaluating the quantum yield weighted average energy-transfer efficiency between a set of tryptophan donors and the ensemble of AO acceptors. The decay of a set of independent donors is given by

$$P(t) = \sum_{i=1}^{N} f_i P_i(t, \tau_i) \tag{10}$$

in which eq 9 is used for $P_i(t,\tau_i)$, f_i is the initial relative intensity of the ith tryptophan, and the sum is over all tryptophans within the protein. Although $P(t)$ depends upon the spatial distribution of the tryptophans, factors such as the intrinsic tryptophan heterogeneity and experimental precision limit the use of the direct measurement of $P(t)$ for determining the tryptophan distribution. We will, therefore, focus on the use of the energy-transfer efficiency (T) for determination of tryptophan distributions.

For a single tryptophan, T is given by

$$T_i = 1 - I_i/I_i^0 \tag{11}$$

in which I_i and I_i^0 are the steady-state intensities of the ith tryptophan in the presence and absence of energy transfer, respectively. In terms of $P_i(t)$ the intensities are

$$I_i = a\int_0^\infty P_i(t)\,dt \tag{12}$$

$$I_i^0 = a\int_0^\infty P_i^\circ(t)\,dt \tag{13}$$

in which a is a proportionality constant and

$$P_i(t) = \exp(-t/\tau_i) \tag{14}$$

As shown in the supplementary material, even when the decay from this single tryptophan is not monoexponential, T_i is virtually independent of the decay constants, and therefore, we may use τ_i in eq 14.

For a protein containing N_T tryptophans, I and I^0 are the sum of the individual tryptophan intensities, and therefore, the multidonor efficiency is

$$T = 1 - \sum_{i=1}^{N_T} I_i / \sum_{i=1}^{N_T} I_i^0 \tag{15}$$

Expressing T in terms of the individual tryptophan efficiencies (eq 11), we have

$$T = \sum_{i=1}^{N_T} \alpha_i T_i \tag{16}$$

in which

$$\alpha_i = I_i^0 / \sum_{i=1}^{N_T} I_i^0 = \epsilon_i Q_i / \sum_{i=1}^{N_T} Q_i \tag{17}$$

ϵ_i and Q_i are the individual tryptophan extinction coefficients and quantum yields, respectively. Since ϵ_i does not vary appreciably with environment (Edelhoch, 1967; Levine & Federici, 1982), we may set all ϵ_i equal, and α_i is, therefore, the fractional quantum yield of the ith tryptophan. Thus, for a heterogeneous set of tryptophans, T is an intensity or quantum yield weighted sum of the individual efficiencies.

Monte Carlo Analysis. To determine the tryptophan distribution from the measured T values, Monte Carlo methods are used to search through a large number of distributions. Each distribution is used to generate a T pattern (efficiency vs. Z_A curve). The calculated (T_p^c) and measured (T_p^m)

patterns are compared by evaluating the error weighted sum of residuals

$$R^2 = \sum_p [(T_p^c - T_p^m)/e_p]^2 \quad (18)$$

in which e_p is the standard deviation of each T_p and the sum is over the different probes (n-AO). To perform the search, single tryptophan efficiencies are calculated at each point in a grid that spans the protein projection on the y, z plane ($\sim$30 $\times$ 80 Å). A set of n ($n \leq N_T$) y, z coordinate pairs is then chosen at random, and for each probe the efficiencies corresponding to these positions are averaged (eq 16). R^2 is evaluated, and the corresponding configuration is sorted in order of decreasing R^2, saving those below a particular cutoff value. Although R^2 correctly reflects the quality of the fit, its absolute value is not defined, e.g., in the sense of χ^2 since the fit is generally underdetermined. This is a consequence of there being more fit parameters [y, z, $R_m(Z_A)$] for multi-tryptophan proteins than measured T values.

Since the problem is underdetermined, configurations deemed acceptable (R^2 below the cutoff) by this procedure are not completely unique. Several different configurations can, therefore, give rise to virtually identical energy-transfer patterns. To display this uncertainty and the results of the Monte Carlo analysis, we have generated tryptophan density maps from the set of acceptable configurations. These maps are formed by examining each acceptable tryptophan configuration, counting (n_i) the occurrence of a tryptophan at each grid point [$y(i)$, $z(i)$] and plotting each of the n_i tryptophans around the ith grid point. Since the area into which the n_i tryptophans are placed around each grid point is constant, the intensity of points is proportional to the probability for the corresponding grid coordinates to occur in an acceptable configuration. In addition to displaying the distribution, the probability densities can be used to calculate the moments of the distribution. In particular, the first and second moments are

$$\langle q \rangle = \sum_{i,j} q_{ij} p_{ij} \quad (19a)$$

$$\mu_q = \sum_{i,j} (q_{ij} - \langle q \rangle)^2 p_{ij} \quad (19b)$$

in which q is either the y or z coordinate and p_{ij} is the probability density at the grid point i, j.

Quantum Yield Distribution. The uncertainty in the quantum yield of each tryptophan in the distribution can lead to considerable ambiguity in the determination of the spatial distribution. In the extreme case, for example, a tryptophan having a quantum yield of zero is invisible in so far as resonance energy transfer is concerned. Although it may be possible experimentally to obtain information about the quantum yield distribution, it is essential that the theory be able to deal with situations in which only the average quantum yield is known. (The average quantum yield can be determined from the number of tryptophans per protein and the fluorescence intensity for a given concentration of protein.) Even in this "worst" case, however, the theory places restrictions on the degree of quantum yield heterogeneity, consistent with the observed energy-transfer efficiencies. This is due to the fact that although fluorescence intensity is proportional to Q, energy transfer is proportional to Q^6. Different $\{\alpha_i\}$, therefore, can yield the same fluorescence intensity, but, in general, give rise to different T values. The restrictions imposed on the quantum yield distribution by the Monte Carlo analysis are demonstrated in the following paper on cytochrome b_5 (Kleinfeld & Lukacovic, 1985).

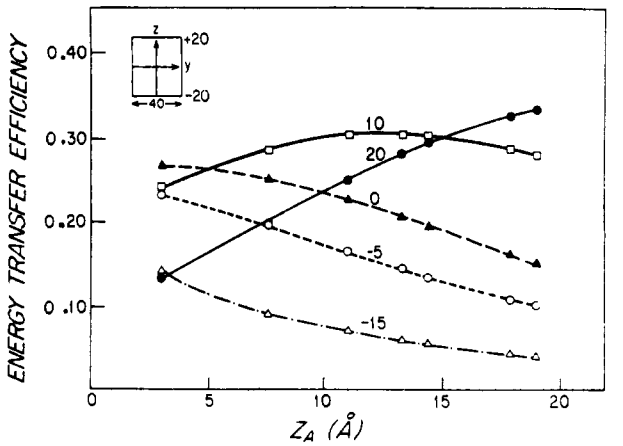

FIGURE 3: Single tryptophan energy-transfer patterns. T values were calculated with an acceptor density of 10 pmol/cm^2, R_0 = 22 Å, a uniform cylinder with R_p = 20 Å, and a tryptophan confined to the central (y = 0) axis of the cylinder. The z position of the tryptophan, indicated on each curve, varied between −15 and +20 Å about the midplane.

The procedure followed in the present study assumes that only the average quantum yield is known, and the initial analysis is performed by setting the quantum yield of each tryptophan equal to the average value. If the actual $\{\alpha_i\}$ is heterogeneous, these conditions may not provide a good fit to the measured T values. The analysis is then repeated by reducing the number of tryptophans and increasing the Q values proportionately until a satisfactory fit is obtained. In effect, this procedure determines a distribution in which each equivalent tryptophan is essentially a quantum yield weighted center of mass of neighboring tryptophans.

Radial Integration Parameter. The radial integration parameter R_m, which is related to the radius of the protein (R_m = R_p + AO radius), can be determined from the energy-transfer measurements, for proteins with one or two tryptophans. To determine the tryptophan distribution and R_m, the T pattern is analyzed by using the Monte Carlo procedure in which the tryptophans are distributed within a cylinder of radius R_m. The radius is varied, and the Monte Carlo analysis is repeated until R^2 is minimized.

RESULTS

Single Tryptophan. In order to simulate the energy-transfer patterns for a single tryptophan-containing protein, calculations were performed for a single tryptophan located along the central axis of a cylinder of 20-Å radius. The results shown in Figure 3 were obtained with $R_0(^2/_3)$ = 22 Å and a density of 10 pmol/cm^2 (about 25 lipids per probe). Large changes in the shape and magnitude of the T patterns are evident for tryptophan positions (y, z) between (0,−15 Å) and (0,20 Å). These variations are experimentally significant since the uncertainty in T is generally less than $\sim$10% for $T > 0.2$.

To evaluate the sensitivity and uniqueness of the Monte Carlo fit, we have analyzed patterns such as those in Figure 3 for several configurations of single tryptophan proteins. Standard deviations for the transfer efficiencies were taken to be 10%. Typical results from this analysis are shown in Figure 4 where the tryptophan density is plotted within the projection of a protein cylinder of radius 20 Å and length 80 Å, for increasing numbers of trial configurations. For a single tryptophan fewer than 10^5 trial configurations are needed to obtain convergence. The tryptophan position determined by this analysis is, to within the accuracy of the grid (2 $\times$ 2 Å), identical with the tryptophan position used to generate the pattern. Thus, these results suggest that the projection of a

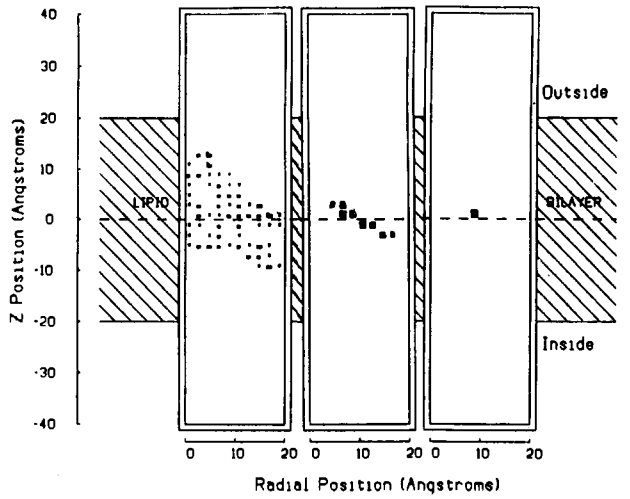

FIGURE 4: Monte Carlo analysis of a simulated single tryptophan experiment. Results are represented by the projection of the tryptophan density on the yz plane. Only the positive y half of the cylinder is shown, since the results are symmetric about the y axis (lack of ϕ dependence). A single tryptophan located at (9,1) was used to generate T values for each AO probe. These simulated efficiencies were analyzed by the Monte Carlo procedure, and the three frames depict the density maps obtained from the best 100 configurations after 5×10^2, 5×10^3, and 5×10^4 randomly chosen single grid (y,z) positions. The search converges to a 2×2 Å grid point at coordinates (9, 1) in less than 5×10^4 trials. The range of R^2 values of the best 100 configurations for each frame is 6–200 for the first, 0.8–6.0 for the second, and a single value of 0.8 for the third.

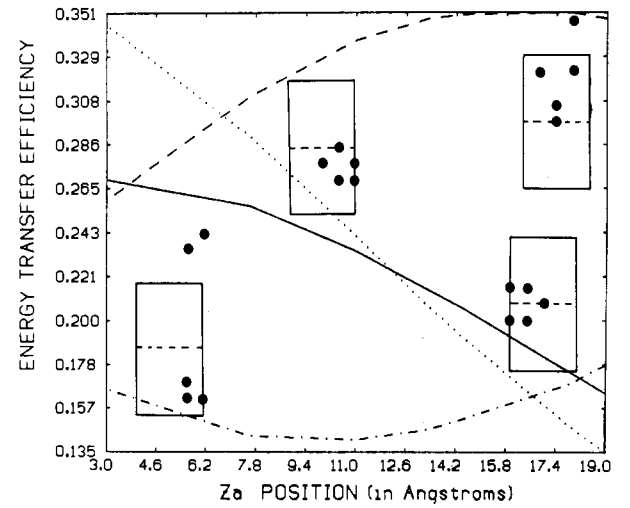

FIGURE 5: T patterns for five tryptophan models. These patterns (efficiency vs. Z_A) were calculated by using eq 16 with $Q_{Trp} = 0.2$, $R_0 = 22$ Å, $R_p = 20$ Å, and $\sigma = 10$ pmol/cm^2. The (yz) projection ($y > 0$ half) of the tryptophan distributions is shown for each model. The outside bilayer leaflet is at the top of the figure, and the dimensions of the projected border are 40 Å vertical and 20 Å horizontal. The (y,z) coordinates of the tryptophan distributions are the following: (—), (0,5), (5,5), (5,0), (5,–5) and (0,–5); (- - -) (10,0), (10,5), (5,15), (15,15), and (15,25); (···) (15,0), (10,–5), (20,–5), (15,–10), and (20,–10); (-·-) (20,35), (15,30), (15,–10), (15,–15), and (20,–15).

single tryptophan can be determined with an uncertainty of less than or equal to 2 Å.

Multiple Tryptophans. Energy-transfer patterns calculated for several multi-tryptophan distributions with a uniform protein cylinder ($R_m = 20$ Å) and equal quantum yields (0.2) are shown in Figure 5. These distributions were chosen to represent broad classes of possible tryptophan configurations, and the coordinates are given in the figure caption. The results illustrate that, in general, the shape and magnitude of the patterns are sensitive to the distributions. Depending upon the tryptophan configuration, the patterns vary from concave

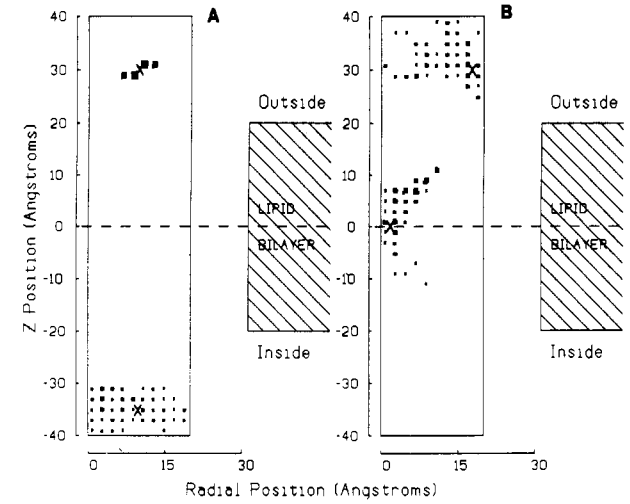

FIGURE 6: Monte Carlo analysis of two tryptophan models. Tryptophan density maps were generated after 10^3 trial configurations (pairs of grid points). The tryptophan positions used to calculate (same parameters as figure 4) the simulated patterns are denoted with an X. (A) Tryptophan coordinates for this model are (10,30) and (10,–35) and the first and second moments are $\langle y \rangle = 10$, $\langle z \rangle = -2.5$, $\mu_y = 0$, and $\mu_z = 32$. The moments obtained from the Monte Carlo analysis were $\langle y \rangle = 8.9$, $\langle z \rangle = -2.2$, $\mu_y = 4.5$, and $\mu_z = 31$, and the range of R^2 values were 0.09–0.54. (B) Tryptophan coordinates for this model are (18,30) and (2,0), and the first and second moments are $\langle y \rangle = 10$, $\langle z \rangle = 15$, $\mu_y = 8$, and $\mu_z = 15$. The moments obtained from the Monte Carlo analysis were $\langle y \rangle = 9.1$, $\langle z \rangle = 18$, $\mu_y = 5.8$, and $\mu_z = 14$, and the range of R^2 values was 0.08–0.47.

downward, to linear, to concave upward. Variations in the magnitude of the energy-transfer efficiencies are substantial compared to expected experimental uncertainties. For example, although the distributions represented by the solid and dashed curves (centrally symmetric and outside skewed distributions, respectively) exhibit similar efficiencies for the deeper probes, the values at the $z \sim 19$ Å position differ by more than 7 standard deviations.

To judge how well the distribution can be determined from the transfer pattern, we generated, as in the case of a single tryptophan, T patterns such as those in Figure 5. These patterns were used as the "experimental" T values for the Monte Carlo analysis. As indicated in Figures 6–8 the multi-tryptophan resolution deteriorates appreciably from the better than 2-Å resolution obtained with a single tryptophan. As greater numbers of tryptophans are considered, it becomes increasingly difficult to distinguish localized density regions corresponding to the position of a particular tryptophan. Since their relative contribution to the total T is reduced, the deterioration in resolution is exacerbated for tryptophans far from the outer leaflet.

In spite of the loss in detailed information for proteins containing more than three tryptophans, it is clear from the results of Figures 6–8 that the gross outline of the distribution can be resolved even for proteins containing many tryptophans. For example, the tryptophan density distribution corresponding to the five tryptophan model A correctly predicts that most of the tryptophans in this model are clustered in a region deep within the outer bilayer and are distributed more peripherally than axially. The results for model B (Figure 8B) correctly reflect the greater spread and the preferential inner bilayer disposition of this distribution. Indeed, in all the simulations we have tried (only a small fraction are shown) the Monte Carlo analysis faithfully returns the mean y, z coordinates of the distribution (see captions of Figures 6–8 for details).

The effect of tryptophan quantum yield (Q_i) heterogeneity on the model distributions of Figures 6–8 has been simulated

Table II: Simulated Quantum Yield Distributions for Five Tryptophan Models[a]

	A[b]		B[b]							
Trp	y	z	y	z	(Q_1)	(Q_2)	(Q_3)	(Q_4)	(Q_5)	(Q_6)
1	3	−3	3	7	0.01	0.10	0.06	0.40	0.20	0.38
2	5	−13	9	9	0.21	0.17	0.19	0.15	0.05	0.25
3	7	9	15	17	0.38	0.33	0.19	0.25	0.30	0.13
4	11	−15	17	15	0.08	0.13	0.31	0.05	0.35	0.00
5	19	−17	11	−5	0.29	0.39	0.25	0.15	0.10	0.25

[a] These distributions were chosen randomly with the requirement that the maximum quantum yield for an individual tryptophan was 0.5 and the average was 0.2. [b] A and B are the tryptophan positions (y, z) of the five tryptophan models of Figure 8.

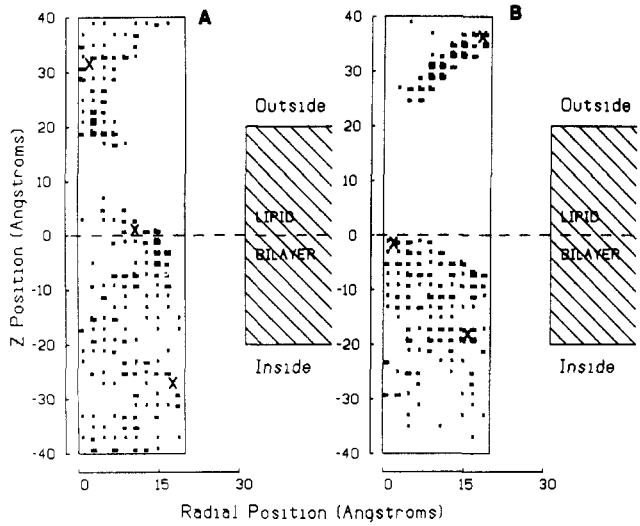

FIGURE 7: Monte Carlo analysis of three tryptophan models. Tryptophan density maps were generated after 10^5 trial configurations (triplets of grid points). The tryptophan positions used to calculate (same parameters as in Figure 5) the simulated patterns are denoted with an X. (A) Tryptophan coordinates for this model are (3,33), (11,1), and (19,−27), and the first and second moments are $\langle y \rangle$ = 11, $\langle z \rangle$ = 2.3, μ_y = 6.5, and μ_z = 25. The moments obtained from the Monte Carlo analysis were $\langle y \rangle$ = 8.7, $\langle z \rangle$ = −1.7, μ_y = 5.5, and μ_z = 23, and the range of R^2 values was 0.11–0.51. (B) Tryptophan coordinates for this model are (19,37), (3,−1), and (17,−19), and the first and second moments are $\langle y \rangle$ = 13, $\langle z \rangle$ = 5.7, μ_y = 7.1, and μ_z = 23. The moments obtained from the Monte Carlo analysis were $\langle y \rangle$ = 10.6, $\langle z \rangle$ = 1.6, μ_y = 5.4, and μ_z = 23, and the range of R^2 values was 0.03–0.19.

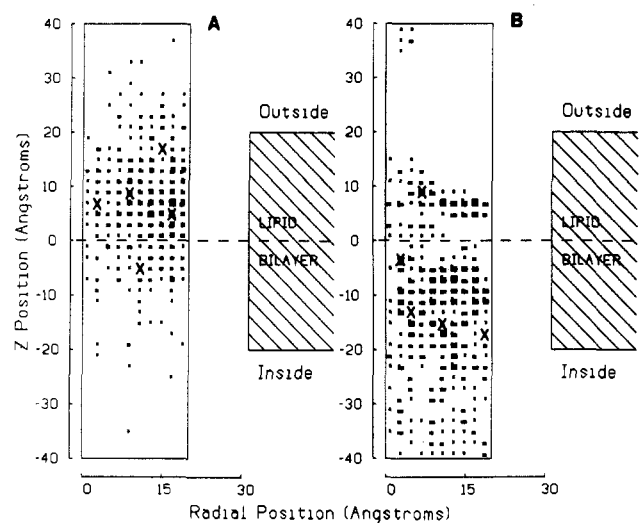

FIGURE 8: Monte Carlo analysis of five tryptophan models. Tryptophan density maps were generated after 5×10^5 trial configurations (quintuplets of grid points). The tryptophan positions used to calculate (same parameters as in Figure 5) the simulated patterns are denoted with an X. (A) Tryptophan coordinates for this model are (3,7), (9,9), (15,17), (17,15), and (11,−5), and the first and second moments are $\langle y \rangle$ = 11, $\langle z \rangle$ = 6.6, μ_y = 4.9, and μ_z = 7.1. The moments obtained from the Monte Carlo analysis were $\langle y \rangle$ = 12.3, $\langle z \rangle$ = 6.4, μ_y = 5.4, and μ_z = 9.3, and the range of R^2 values was 0.06–0.48. (B) Tryptophan coordinates for this model are (7,9), (3,−3), (5,−13), (11,−15), and (19,−17), and the first and second moments are $\langle y \rangle$ = 9, $\langle z \rangle$ = −7.8, μ_y = 5.7, and μ_z = 9.7. The moments obtained from the Monte Carlo analysis were $\langle y \rangle$ = 10.4, $\langle z \rangle$ = −10.7, μ_y = 5.5, and μ_z = 14, and the range of R^2 values was 0.09–0.42.

by choosing at random, six sets of quantum yields (Table II). These values were used to calculate T patterns for each model, according to eq 16. The patterns were analyzed by attempting to fit with n tryptophans (with n between 2 and 5), in which the quantum yields of each of the n tryptophans were equal and chosen so that the average quantum yield of the trial configuration was the same as that of the model used to simulate the T patterns. In Figure 9 results obtained with n = 4 are presented for those $\{Q_i\}$ values yielding the greatest variation in the tryptophan density maps. These results indicate that while extreme variations in $\{Q_i\}$ do affect the details of the tryptophan spatial distribution, the essential features are conserved, and in particular, the quantum yield weighted average position of the distributions is correctly determined. Although these examples are not intended to be exhaustive, they do suggest that, in many cases, even complete lack of information about $\{Q_i\}$ will not obscure the essential features of the spatial distribution. Clearly for two or three tryptophans, variations in $\{Q_i\}$ will result in more significant changes in the determined distribution. In these cases, however, $\{Q_i\}$ is far more amenable to experimental determination.

Energy transfer is also a function of the protein's radial parameter. Details of this dependence were investigated to determine if radial effects could be deconvoluted from the tryptophan distribution. For the case of a single tryptophan, the tryptophan location and protein radial parameter can be uniquely determined from the transfer efficiencies as demonstrated by Fleming et al. (1979) and our own study in the following paper (Kleinfeld & Lukacovic, 1985). To examine the effect of protein radius in multi-tryptophan proteins, models of two to five tryptophans were chosen, and T patterns were calculated for various R_m values. Each of these simulated patterns, calculated by using a particular R_m, was analyzed by the Monte Carlo method for R_m values between 8 and 26 Å (data not shown). For two tryptophan proteins R^2 values exhibit a minimum in the vicinity of the actual R_m value; however, this minimum is less pronounced than in the case of a single tryptophan. For proteins with more than two tryptophans the quality of fit and the tryptophan distribution in the z direction is independent of R_m over a wide range of R_m values. Thus, in the general case it will not be possible to determine R_m or the absolute y coordinates of the distribution without additional information about the protein's radius. The determination of the z projection of the distribution will, however, not be affected by this lack of R_m information.

Discussion

It has been demonstrated that the tryptophan–AO model of energy transfer should be an effective method of obtaining information about the spatial distribution of tryptophan residues in membrane proteins. For a single tryptophan-con-

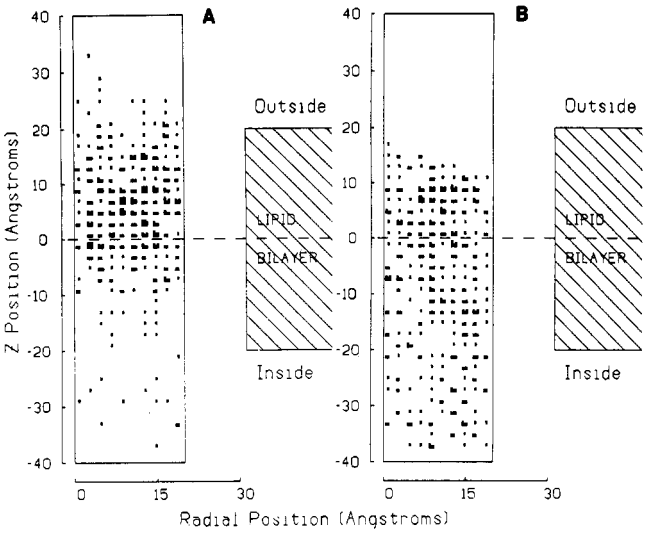

FIGURE 9: Monte Carlo analysis of five tryptophan models with heterogeneous quantum yield distribution. The parameters used to simulate the patterns (except for the quantum yields) and the representation of the results are the same as in Figure 8. (A) The simulation was performed with the model of Figure 8A and the (Q_6) distribution of Table II. The moments of the simulated distribution are $\langle y \rangle = 8$, $\langle z \rangle = 5.8$, $\mu_y = 4.2$, and $\mu_z = 6.9$. The moments obtained from the analysis were $\langle y \rangle = 10.6$, $\langle z \rangle = 4.7$, $\mu_y = 5.7$, and $\mu_z = 10.7$, and the range of R^2 values was 0.03–0.15. (B) The simulation was performed with the model of Figure 8B and the (Q_4) distribution of Table II. The moments of the simulated distribution are $\langle y \rangle = 7.1$, $\langle z \rangle = -4.2$, $\mu_y = 5.4$, and $\mu_z = 9.3$. The moments obtained from the analysis were $\langle y \rangle = 10.1$, $\langle z \rangle = -7.2$, $\mu_y = 5.6$, and $\mu_z = 14$, and the range of R^2 values was 0.02–0.16.

taining protein the location can be determined with a precision of about 2 Å; for two and three tryptophan proteins the resolution, although not of this quality, is still sufficient to resolve individual residues. Individual residues cannot, in general, be resolved for proteins with larger numbers of residues; however, it is possible to determine the essential features of the distribution such as the first and second moments. Information of this kind can be quite useful, for example, in assessing the proposed model (Engelman et al., 1982) for threading the primary sequence of bacteriorhodopsin through the membrane.

In the supplementary material it is shown that the determination of the spatial distribution is not particularly sensitive to the tryptophan–AO orientation factor, K^2. The determination of the distribution does, in general, depend on quantum yield heterogeneity. It was argued, however, that even when only the average tryptophan quantum yield is known, the model and the energy-transfer mechanism restrict the possible solutions. Furthermore, literature values for the tryptophan quantum yields [see, for example, Burstein et al. (1973)] suggest that the range of tryptophan Q values is restricted to be <0.4, and experimental methods can help determine a protein's quantum yield distribution, $\{Q_i\}$. *N*-Bromosuccinamide can be used to selectively and stoichiometrically eliminate both the fluorescence and absorbance of tryptophan and thereby, in principle, allow the determination of $\{Q_i\}$ (Fleming & Strittmatter, 1978). Agents which quench tryptophan fluorescence at close range and which themselves are localized (charged and fatty acid spin-label quenchers, for example) can be used to help correlate $\{Q_i\}$ and the spatial distribution of tryptophan. Quantum yield heterogeneity can be explicitly accounted for in the analysis by randomly choosing $\{Q_i\}$ in eq 17, a reasonable possibility if experimental results could be used to place limits on the range of $\{Q_i\}$ variation.

Calculations in the present study were based on the assumption that all probes are in the outer bilayer leaflet. This restriction is, of course, not fundamental since the theory readily accomodates a finite partition between the two bilayer halves. The assumption of inside/outside partition = 0 is based upon observations in red cells (Shaklai et al., 1977; Eisinger & Flores, 1982). A disadvantage of the probe's restriction to the outer bilayer leaflet is that the resolution of tryptophan locations in the inner leaflet and beyond is seriously compromised. Considerable improvement in resolution would, therefore, result if conditions could be found for which these or similar probes could be made to flip to the inner leaflet.

Numerous studies have examined the question of structural perturbation by membrane probes (Radda, 1975; Cadenhead et al., 1977; Ashcroft et al., 1980). It is, however, unclear how protein structure will be affected by probes such as the AO fatty acids which do not act covalently and are used in concentrations less than 10 mol %. Several lines of evidence from our own experimental studies suggest that the protein structure is not significantly perturbed by these probes (Kleinfeld et al., 1982). We have found that, in the case of the anion transport protein, band 3, the AO probes have no detectable effect on anion exchange, even at concentrations 4-fold greater than those used in the energy-transfer experiments. The tryptophan distribution and protein profile obtained in experimental studies were found to be invariant with probe density. Finally, fluorescence properties of the probes themselves such as lifetime, quantum yield, and anisotropy were found to be independent of their membrane-phase concentration.

AO probes have been used to measure resonance energy transfer from membrane-associated tryptophan by Haigh et al. (1979) using gramicidin and the tryptophan-coupled fatty acid *N*-stearoyltryptophan. Contrary to the conclusions reached here, however, these authors concluded that tryptophan location could not be assessed by this method. There are several experimental and theoretical reasons for this disagreement. The T values calculated by Haigh et al. (1979), although smaller than our own (they used $R_0 = 19$ Å), are not insignificant (>0.14). It is surprising, therefore, that their experimental efficiencies are so much smaller than these calculated values [Figure 1 of Haigh et al. (1979)]. In their studies, carried out in multilamellar liposomes of dimyristoyl-PC at 20 °C (below the main gel to liquid-crystalline phase transition at 24 °C), Haigh et al. (1979) observed that the indole ring of tryptophan quenched AO fluorescence. This effect, presumably, accounted for the small observed energy-transfer efficiencies.

We could not confirm such quenching in studies of red cell ghosts and in egg PC vesicles reconstituted with cytochrome b_5, band 3, or bacteriorhodopsin (Kleinfeld et al., 1982). Studies have also been carried out with gramicidin in small unilamellar vesicles of dimyristoyl-PC at 32 °C (Connolly et al., 1985). Briefly, we found (1) both tryptophan quenching and sensitized emission yield identical transfer efficiencies and (2) the lifetimes and quantum yields of the probes are unaffected by the presence of protein. The reason for the observed small efficiencies in the study of Haigh et al. has probably to do with the use of multilamellar vesicles coupled with the lack of appreciable AO interbilayer movement (Storch and Kleinfeld, unpublished results). Thus, in their study, vesicles were preformed with donor so that the donor tryptophan was distributed throughout the lamellae. The probe, however, was added externally, and therefore, very little of the donor tryptophan was within R_0 of the AO acceptor.

Supplementary Material Available

Two appendixes (A and B) in which the effect of dipole orientation (A) and tryptophan decay heterogeneity (B) are

evaluated for the tryptophan–AO energy-transfer system (14 pages). Ordering information is given on any current masthead page.

Registry No. Trp, 73-22-3; 2-AS, 78447-89-9; 3-AS, 86637-08-3; 6-AS, 67708-95-6; 7-AS, 78447-90-2; 9-AS, 69243-44-3; 10-AS, 56970-51-5; 12-AS, 30536-60-8; 16-AP, 64821-29-0.

References

Ashcroft, R. G., Thulborn, K. R., Smith, J. R., Coster, H. G., & Sawyer, W. H. (1980) *Biochem. Biophys. Acta 602*, 299–308.

Burstein, E. A., Vedenkina, N. S., & Ivkova, M. N. (1973) *Photochem. Photobiol. 18*, 263–279.

Cadenhead, D. A., Kellner, M. J. B., Jacobson, K., & Papahadjopoulos, D. (1977) *Biochemistry 16*, 5386–5391.

Chalpin, D. B., & Kleinfeld, A. M. (1983) *Biochim. Biophys. Acta 731*, 465–474.

Connolly, A. J., Boni, L. T., & Kleinfeld, A. M. (1985) *Biophys. J. 47*, 431a.

Dale, R. E., & Eisinger, J. (1975) in *Biochemical Fluorescence* (Chen, R. F. & Edelhoch, H., Eds.) Vol. 1, pp 115–284, Marcel Dekker, New York.

Dale, R. E., Eisinger, J., & Blumberg, W. E. (1979) *Biophys. J. 26*, 161–193.

Dewey, T. G., & Hammes, G. C. (1980) *Biophys. J. 32*, 1023–1034.

Edelhock, H. (1967) *Biochemistry 6*, 1948–1954.

Eisinger, J., & Flores, J. (1982) *Biophys. J. 37*, 6–7.

Eisinger, J., Blumberg, W. E., & Dale, R. E. (1981) *Ann. N.Y. Acad. Sci. 366*, 155–175.

Eisinger, J., Flores, J., & Salhany, J. M. (1982) *Proc. Natl. Acad. Sci. U.S.A. 79*, 408–412.

Engelman, D. M., Henderson, R., Mclachlan, A. D., & Wallace, B. A. (1980) *Proc. Natl. Acad. Sci. U.S.A. 77*, 2023–2027.

Engelman, D. M., Goldman, A., & Steitz, T. A. (1982) *Methods Enzymol. 88*, 81–88.

Estep, T. N., & Thompson, T. E. (1979) *Biophys. J. 26*, 195–207.

Fleming, G. R., Morris, J. M., Robbins, R. J., Woolfe, G. J., Thistlethwaite, P. J., & Robinson, G. W. (1978) *Proc. Natl. Acad. Sci. U.S.A. 75*, 4652–4656.

Fleming, P. J., & Strittmatter, P. (1978) *J. Biol. Chem. 253*, 8198–8202.

Fleming, P. J., Koppel, D. E., Lau, A. L. Y., & Strittmatter, P. (1979) *Biochemistry 18*, 5458–5464.

Förster, Th. (1948) *Ann. Phys. 2*, 55–75.

Fung, B. K. K., & Stryer, L. (1978) *Biochemistry 17*, 5241–5248.

Gall, C. M., Cross, T. A., Diverdi, J. A., & Opella, S. J. (1982) *Proc. Natl. Acad. Sci. U.S.A. 79*, 101–105.

Haas, E., Katchalski-Katzir, E., & Steinberg I. Z. (1978) *Biochemistry 17*, 5064–5070.

Haigh, E. A., Thulborn, K. R., & Sawyer, W. H. (1979) *Biochemistry 18*, 3525–3532.

Henderson, R., & Unwin, P. N. T. (1975) *Nature (London) 257*, 23–32.

Khorana, H. G., Gerber, G. E., Herlihy, W. C., Gray C. P., Anderegg, R. J., Nihei, K., & Biemann, K. (1979) *Proc. Natl. Acad. Sci. U.S.A. 76*, 5046–5050.

Kinsey, R. A., Kintanar, A., & Oldfield, E. (1981) *J. Biol. Chem. 256*, 9028–9036.

Kleinfeld, A. M., & Lukacovic, M. F. (1985) *Biochemistry* (following paper in this issue).

Kleinfeld, A. M., Lukacovic, M. F., Matayoshi, E. D., & Holloway, P. (1982) *Biophys. J. 37*, 146a.

Koppel, D. E., Fleming, P. J., & Strittmatter, P. (1979) *Biochemistry 18*, 5450–5457.

Kutchai, H., Chandler, L. H., & Zavoico, G. B. (1984) *Biochim. Biophys. Acta 736*, 137–149.

Lakowicz, J. R., & Weber, G. (1980) *Biophys. J. 32*, 591–601.

Lakowicz, J. R., Maliwal, B. P., Cherek, H., & Balter, A. (1983) *Biochemistry 22*, 1741–1752.

Lesslauer, W., Cain, J. E., & Blasie, J. K. (1972) *Proc. Natl. Acad. Sci. U.S.A. 69*, 1499–1503.

Levine, R. L., & Federici, M. M. (1982) *Biochemistry 21*, 2600–2606.

Matayoshi, E. D., & Kleinfeld, A. M. (1981) *Biophys. J. 35*, 215–235.

Munro, I., Pecht, I., & Stryer, L. (1979) *Proc. Natl. Acad. Sci. U.S.A. 76*, 56–60.

Ovchinnikov, Yu. A., Abdulaev, N. G., Feigina, M. Yu., Kiselev, A. V., & Lobanov, N. A. (1979) *FEBS Lett. 100*, 219–224.

Podo, F., & Blasie, J. K. (1977) *Proc. Natl. Acad. Sci. U.S.A. 74*, 1032–1036.

Radda, G. K. (1975) *Methods Membr. Biol. 4*, 97–188.

Ross, J. B. A., Rousslang, K. W., & Brand, L. (1981a) *Biochemistry 20*, 4361–4369.

Ross, J. B. A., Schmidt, C. J., & Brand, L. (1981b) *Biochemistry 20*, 4369–4377.

Shaklai, N., Yguerabide, J., & Ranney, H. M. (1977) *Biochemistry 16*, 5585–5592.

Vincent, M., Foresta, B., Gallay, J., & Alfsen, A. (1982) *Biochemistry 21*, 708–716.

Wolber, P. K., & Hudson, B. S. (1979) *Biophys. J. 28*, 197–210.